

Search for an electric charge of the neutron

C. Siemensen,^{1,*} C. Düsing,¹ P. Geltenbort,² C. Giebel,¹ T. Reich,¹ and C. Plonka¹

¹*Institute of Nuclear Chemistry, Johannes Gutenberg University Mainz,
Fritz-Strassmann-Weg 2, 55128 Mainz, Germany*

²*Institut Laue-Langevin, 71 Avenue des Martyrs, 38000 Grenoble, France*



(Received 31 January 2017; published 15 March 2018)

The electrical neutrality of the neutron is linked to the electric charge quantization. It is not understood yet if the electric charge is quantized or not. Since the discovery of the neutron, many attempts have been made to measure its electric charge q_n directly and indirectly. We present a method to search for a possible q_n by means of an optical setup using ultracold neutrons. In a first run, a statistical sensitivity of $\delta q_n = 2.4 \times 10^{-20} e/\sqrt{\text{day}}$ is achieved. Possible improvements to increase this sensitivity down to $\delta q_n \approx 1 \times 10^{-21} e/\sqrt{\text{day}}$ are found and discussed.

DOI: 10.1103/PhysRevD.97.052004

I. INTRODUCTION

The electric charge quantization (ECQ) is still one of the most weighty mysteries in physics [1]. It is not understood why electric charges should be an integral number of some smallest fraction. Dirac tried to fix the problem of ECQ by introducing magnetic monopoles [2]. Mathematically, ECQ is not inherent in experimentally well-confirmed theories like quantum electrodynamics (QED) or the standard model (SM) of particle physics. We will take a closer look at the minimal standard model (MSM; minimal refers to zero neutrino masses [3]) as this theory seems very appealing from a particle physics point of view. The MSM contains three generations of fermions. Any generation can be condensed to a multiplet, namely

$$\left(\begin{pmatrix} \nu_L \\ e_L \end{pmatrix}, e_R, \begin{pmatrix} u_L \\ d_L \end{pmatrix}, u_R, d_R \right).$$

Such a multiplet contains seven hypercharges. Right-handed particles have the index R , left handed particles L . As there are three generations, we have 21 hypercharges to be determined. Massive fermions achieve their mass by a Yukawa coupling to the Higgs field. This coupling must be invariant under $U(1)$ transformations. Thus, left- and right-handed particles must carry the same electric charge. Right-handed particles are determined by their left-handed partners. Therefore, the number of undetermined hypercharges is reduced to twelve. The electric charge Q and the weak hypercharge Y_W are related via the weak isospin component T_3 :

$$Q = T_3 + Y_W/2. \quad (1)$$

The electric charge in one fermion doublet only differs in their weak isospin component T_3 , while the weak hypercharges Y_W stay the same. Down-type fermions are determined by their up-type partners. This limits our set of free parameters to only six. All quark flavors mix via the Cabbibo-Kobajashi-Maskawa (CKM) matrix. It has been shown experimentally that all elements of the CKM matrix are nonzero [4]. This means that all quarks of up-type and all quarks of down-type must carry the same hypercharge and, hence, all quark generation charges are determined by only one quark hypercharge. Thus four free parameters for the weak hypercharge remain. Taking into account the so-called anomaly cancellations, we obtain a few more constraints [5]. Anomaly cancellations are needed to fulfill the Ward identities in quantum field theories to make the theory renormalizable. The easiest kind of anomaly is a triangle anomaly as sketched in Fig. 1. It is sufficient to take only those anomalies into account for cancellation, as higher order anomalies will then cancel as well. This statement is known as the Adler-Bardeen theorem [6,7]. The general form of an anomaly in the (minimal) standard model is [8]

$$\mathcal{A}_{\mu\nu}^{\text{SM}} \propto \text{tr} \gamma_5 T^a \{T^b, T^c\} \cdot \mathcal{A}_{\mu\nu}^a. \quad (2)$$

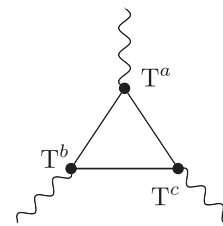


FIG. 1. A general triangle anomaly. Three gauge bosons couple via a fermion loop. T^x denote the generators of the respective groups for the coupling of the vector bosons.

*c.siemensen@uni-mainz.de

T^x are the generators of the respective groups for the coupling of our vector bosons (e.g. $Y \in U(1)$ for the hypercharges, $\tau \in SU(2)$ for the weak interaction). γ_5 represents the handedness of the weak interaction. $\mathcal{A}_{\mu\nu}^a$ is the anomalous contribution in the Abelian case, which is in general nonzero. The anticommutator arises from the sum over both impulse swirls in the fermion loop. Only three types of anomalies do not vanish directly and thus yield additional constraints for the hypercharges [5]:

- (1) Coupling of a photon with two Z-bosons (f_L denotes all left-handed fermions): $\text{tr}Y\{\tau^b, \tau^c\} = \frac{\delta^{bc}}{2} \sum_{f_L} Y_{f_L} \stackrel{!}{=} 0 \Leftrightarrow Q_{\nu 1} + Q_{\nu 2} + Q_{\nu 3} + 9Q_d = -3$. The sum of all neutrino charges and the down type quark charges should add up to -3 elementary charges.
- (2) Three photons (f denotes all fermions): $\text{tr}Y^3 = \sum_f Y_f^3 \stackrel{!}{=} 0 \Leftrightarrow Q_{\nu 1}^3 + Q_{\nu 2}^3 + Q_{\nu 3}^3 = 0$.
- (3) Two gravitons and one photon: $\text{tr}Y = \sum_f Y_f \stackrel{!}{=} 0 \Leftrightarrow Q_{\nu 1} + Q_{\nu 2} + Q_{\nu 3} = 0$.

We have three independent equations for four free hypercharges. Currently, the charges of particles in the MSM are just assigned in the known way (e.g. third elementary charge for quarks etc.). But why should nature choose especially this assignment? In general, the hypercharge and respectively the electric charge is not determined in the MSM. In this discussion we only considered the MSM, where neutrinos are assumed to be massless. It is possible to explain ECQ within the standard model only if massive Majorana neutrinos exist [3,9]. Thus, small charge deviations of e.g. neutrons or neutrinos [10], atoms and molecules [11] or even neutral bulk matter from charge zero are possible. For this reason the determination of the free neutron electric charge plays a key role in answering the question whether ECQ does exist or not.

II. THE SEARCH FOR AN ELECTRIC CHARGE OF THE NEUTRON

A. Current status

Since the discovery of the neutron, there have been several attempts to determine its electric charge directly. The results for the upper limit observed in direct measurements of the electric charge of the free neutron are subsumed in Fig. 2.

The sensitivity of the experiments scales with the velocity of the neutrons. The three limits in the upper right corner were reviewed by Shull *et al.* [15]. Over the last decades, many experiments were conducted to determine the electric charge of bulk matter, molecules, atoms, free neutrons or neutrinos. The most recent ones were the following:

- (i) The electric charge of bulk matter has been determined by means of magnetically levitated steel spheres by Marinelli *et al.* The difference between

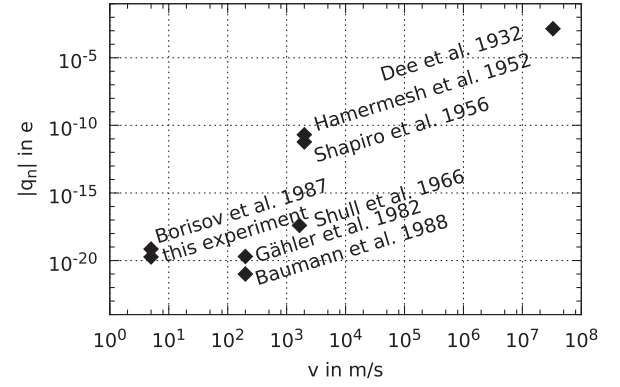


FIG. 2. Upper limits for the electric charge of the free neutron vs the mean velocity of the neutrons in the respective experiments. The experiments by Dee *et al.* [12] and Hamermesh *et al.* [13] were scattering experiments. Shapiro, Shull, Gähler, Borisov, Baumann [14–18] and this work used the deflection of a neutron beam in an electric field.

the charge of the protons and of the electrons was $(0.8 \pm 0.8) \times 10^{-21} e$ [11].

- (ii) The neutron charge was determined by exciting SF_6 in a spherical capacitor with an ac-electric field to $(-0.1 \pm 1.1) \times 10^{-21} e$ by Bressi *et al.* [19].
- (iii) The deflection of cold neutrons at velocities about ≈ 200 m/s in an optical system in a strong dc-electric field yielded $q_n = (-0.4 \pm 1.1) \times 10^{-21} e$ by Baumann *et al.* [18].
- (iv) From the bunching of neutrinos from the supernova SN1987A a limit for the charge of neutrinos of $q_\nu < 10^{-17} e$ [20] could be deduced.

So far, the experiment of Baumann *et al.* [18] still holds the best limit for the electric charge of the free neutron. Recently, several new approaches for the determination of the free neutron electric charge have been proposed:

- (i) Spin interferometry with cold neutrons with velocities around 100 m/s [21].
- (ii) Ramsey spectroscopy of gravitational quantum states of ultracold neutrons [22].
- (iii) An optical method with ultracold neutrons (velocities $\lesssim 7.6$ m/s), described hereafter [23].

All these experiments aim to increase the sensitivity δq_n of at least 1 order of magnitude and to determine the free neutron electric charge at a level of $\approx 10^{-22} e$. Besides using free neutrons there are also new approaches for probing the electric charge of bulk matter by means of a torsion pendulum [24] or atomic interferometry [25].

B. Optical method

Our method described here is based on an experiment which has been performed in the late 1980s [17] with ultracold neutrons (UCN). UCN have kinetic energies below 300 neV or velocities below 7.6 m/s. They will

be reflected by surfaces with a higher Fermi potential¹ compared to their kinetic energy [26] (e.g. for nickel $V_F \approx 250$ neV). Such surfaces can have e.g. specific curvatures and thus optical imaging with UCN is possible. Due to their magnetic moment, UCN can also be reflected from magnetic fields. The gravitational interaction causes parabolic flight paths of the UCN. UCN can be trapped in material bottles or magnetic fields for long times (about time scales of the lifetime of the free neutron τ_n). They are well suited for high precision experiments like lifetime measurements [27] or searches for a permanent electric dipole moment [28]. UCN can be produced in different ways. We will briefly describe the production of UCN at the UCN facility at PF2² at the Institut Laue-Langevin (ILL) in Grenoble, France: Neutrons from a high flux reactor are moderated in a liquid deuterium vessel and transferred via a neutron guide to a turbine. Here, the neutrons have velocities around 50 m/s. Elastic scattering at the moving turbine blades slow most of the neutrons down to the UCN spectrum [29]. The UCN guide from the turbine can be closed by a pneumatic shutter.

UCN are suitable for a search of a possible electric charge of the free neutron, because

- (i) they are slow, promising long durations of stay in electric fields and
- (ii) they can be used to realize optical imaging, promising a higher sensitivity than just the deflection of a single beam.

The first determination of the electric charge of the neutron with UCN yielded

$$q_n = (-4.3 \pm 7.1) \times 10^{-20} e \quad (3)$$

in a three days measurement by Borisov *et al.* [17].

They used an “optical method,” which is sketched in Fig. 3. The UCN pass via an input guide (e) through an input grating (a) into an optical system. They are reflected by a cylindrical mirror (b) of curvature R in a distance $d = R$ in the direction of an exit grating (c). Gravity acts in the z direction and, hence, does not influence the trajectories of the UCN in the x and y direction. Thus, the optical system can be treated with ray optics: the cylindrical mirror images the input grating (a) onto the position of the exit grating (c) (see green beam in Fig. 3). During their path through the optical system, the UCN can be exposed to a force (e.g. caused by an electric field E) perpendicular to the optical axis. The image of the input grating (a) on the exit grating (c) will be shifted by Δx (see red dashed beam in Fig. 3). The polarity of this force is reversed periodically for a differential measurement. The exit grating (c) can be moved perpendicular to the optical axis along the x direction. Thus, a modulation in the count rate n of the detector (d) could be achieved (see Fig. 5). The exit grating (c) is set to the position

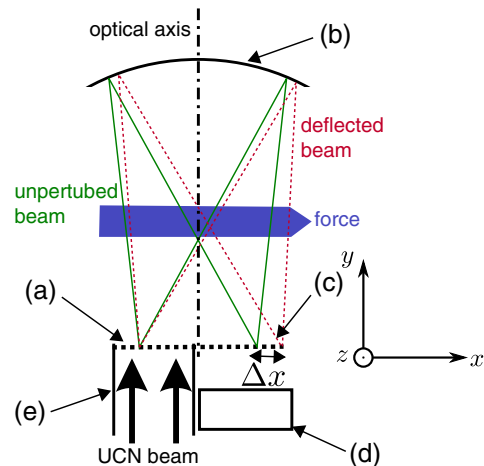


FIG. 3. Optical method for determining small forces on UCN beams: input grating (a), cylindrical mirror (b), exit grating (c), detector (d) and UCN input guide (e).

of the steepest slope $\partial_x n$ of the modulation curve. This is the bias point, which is determined by a linear fit. If the neutrons are deflected due to a force along their flight path, this deflection can be measured via

$$\Delta x = \frac{\Delta n}{\partial_x n}, \quad (4)$$

where Δn is the change in count rate after the reversal of the force $\Delta F = F^+ - F^-$ in a differential measurement:

$$\Delta x = \frac{\Delta F t^2}{2m_n}. \quad (5)$$

t is the time of flight for the neutrons through the electrode system and m_n is the mass of the neutron. In the presence of an electric field, the charge of the neutron q_n can be directly assigned, if $\Delta F = \Delta E q_n$:

$$q_n = \frac{2m_n}{\Delta E t^2} \frac{\Delta n}{\partial_x n}. \quad (6)$$

ΔE is the difference of the electric field after reversing the polarity.

Recapitulating, this apparatus acts as a projector with UCN instead of light. An input grating is imaged onto an exit grating with a cylindrical mirror. A shift of the neutron beam inside the optical system results in a shift of that image. This shift can be determined precisely from the change in the count rate in the detectors behind the output grating. We constructed a first test apparatus as a proof of concept in 2010 [30]. Since then, many changes have been made to increase the sensitivity. These changes are described in detail in [23].

C. Apparatus

The optical method described above has been realized by the apparatus shown in Fig. 4.

The neutrons (dashed line) pass the input grating (a), are reflected by the cylindrical mirror (b) in a distance of

¹E. Fermi found that the scattering of slow neutrons in matter could be described by an effective potential, which is repulsive for most materials.

²Physique fondamentale.

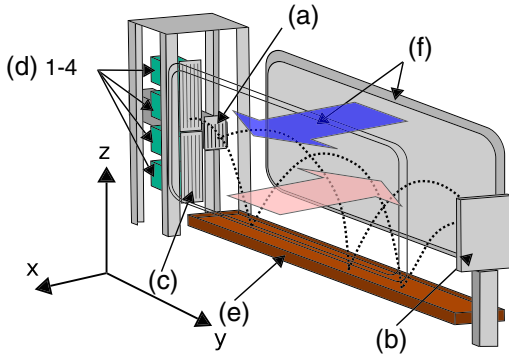


FIG. 4. Schematic view of our apparatus: input grating (a), cylindrical mirror (b), exit gratings (c), detectors d ((d 1) is the upper detector, (d 4) the lower detector), horizontal mirror (e), electrodes (f). The other electrode is only outlined. The two bold arrows denote the different field directions dependent of the polarity. The dashed line represents the path of a neutron.

1500 mm (which is also the radius of the mirror curvature) and imaged onto the exit gratings (c). The cylindrical mirror (b) has the dimensions of 150 mm in height and 100 mm in width. It is coated with 500 nm of NiMo (85/15 wt. %). The gratings (a), (c) are machined of 0.2 mm thick Ni-foil by laser cutting with a slit width of 0.4 mm and a spacing of 1.1 mm. The foils are mounted on rigid aluminium frames. The exit grating (c) is divided into two parts (an upper grating and a lower grating). Both gratings can be moved independently in the x direction by motorized high precision linear stages. This enables a differential measurement by putting one exit grating onto the positive slope and the other exit grating onto the negative slope of the modulations (see Fig. 5). Thus, the effect of UCN flux fluctuations could be neglected. At the rear of the exit gratings, four Li-doped glass scintillators (GS 20, Saint-Gobain) coupled to photomultiplier tubes (detectors (d 1)–(d 2) for the upper exit grating, detectors (d 3)–(d 4) for the lower exit grating) detect the passed neutrons. We use a basin filled with liquid Fomblin (e) as horizontal reflector to confine the UCN in the z direction. This geometry ensures that the neutrons are reflected ≤ 3 times on the liquid surface only.³ Thus, we can reduce perturbing effects by surface distortions like surface vibrations, waves, roughness and tilts of the horizontal mirror.

So far, Fomblin has been used as coating for storage experiments (e.g. [31]). As horizontal mirror, we used liquid Fomblin (Y–HVAC 140/13, Solvay). It has a low vapor pressure, is extremely viscous [32] and has a high durability in high electric fields [33]. It has an intrinsic roughness of ≈ 5 Å. We measured a dielectric constant of $\epsilon(23^\circ\text{C}) \approx 2.4$, which is not dependent on the electric field in the range of 20–640 kV/m.

Along the optical path two electrodes (f) separated by a 10 cm gap generate the electric field E . They were machined of nonmagnetic stainless steel (type 1.4301) with a thickness of 10 mm. The dimensions are

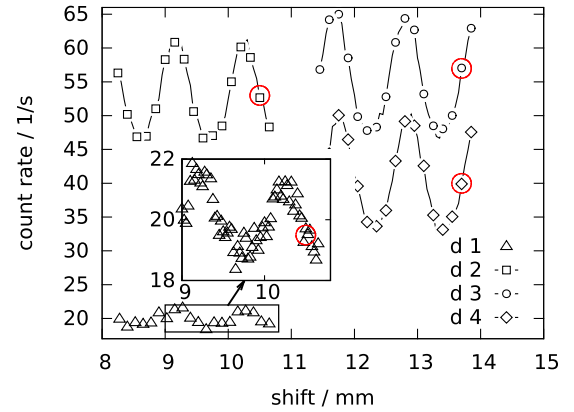


FIG. 5. Modulation curves in count rate vs shift of the exit gratings along the x direction. The bias points are highlighted red. Detectors 1 and 2 are covered by the upper grating, detectors 3 and 4 by the lower grating.

$1250 \times 310 \text{ mm}^2$. The surface roughness is $R_a \approx 1 \mu\text{m}$. They are coated with acrylic paint to remove UCN that hit the electrodes by upscattering.⁴ Grounded electrodes shield the gratings and the horizontal mirror (not shown). Tests showed that this setup could be operated reliably for several minutes up to 1.6 MV/m without discharges.

III. RESULTS

We carried out our measurements at the Institute Laue-Langevin (France, Grenoble) in November–December 2014 at the “UCN” beam port at PF2 [29]. After the apparatus was set up and all optical parts aligned, we measured the modulation curves (see Fig. 5). The modulation curves are on one hand a confirmation of proper operation of the optical system. On the other hand they are needed to determine the slope $\partial_x n$ of the bias points and to investigate background effects. Before starting with the charge measurement, we investigated the background thoroughly and tried to reduce it by placing absorbers and reflectors at different positions in our experiment.

A. Background measurement

Our background is defined as the count rate at the minimum of each modulation curve (see Fig. 5). The reduction of the background signal is crucial for the sensitivity of our apparatus. The statistical uncertainty scales with the square root of the count rate \sqrt{n} [see Eq. (8)]. We were able to figure out the different contributions to our background like trapped or misled⁵ UCN, upscattered UCN, thermal neutrons from the UCN turbine, the reactor and intrinsic background of the detectors. Those sources were determined by successively covering the

³For more information see [23].

⁴Upscattering describes the incoherent scattering, e.g. on hydrogen, of UCN resulting in an enhancement to energies above the UCN spectrum.

⁵e.g. due to reflection on nonoptical parts.

TABLE I. Contributions to the background signal for each detector. Each contribution is given in percent of the count rate in the modulation minimum (see Fig. 5) for each detector.

Detector #	UCN	Upscattering	Turbine	Reactor	Intrinsic
1	24.0%	44.7%	4.2%	0.2%	27.1%
2	43.1%	42.1%	2.8%	0.1%	12.0%
3	38.3%	44.8%	4.3%	0.2%	12.6%
4	28.8%	41.0%	6.7%	0.3%	23.5%

detectors with thin Ni-foils (stopping UCN), closing the shutter of our turbine exit (background from thermal neutrons from the turbine and the reactor), closing the main shutter to the reactor (background from thermal neutrons from the reactor) and analyzing the neutron spectra (intrinsic background of the detectors), respectively.

In Table I, one can see that the majority of the background is caused by upscattered UCN and misled or trapped UCN, respectively. This background could be further reduced, e.g. by coating the electrode surface with absorbing material like titanium instead of upscattering material. In the future, the amount of misled UCN could be reduced by adding other absorbing materials around the optical system to absorb trapped UCN in the vacuum chamber.

B. Charge measurement

We started the measurements of the neutron electric charge in mid November 2014. We determined the positions and the slopes of the bias points in the modulation curves shown in Fig. 5.

The slopes and the positions of the bias points were checked every few days during the experiment and after completion of the charge measurement. The parameters of our experiment are shown in Table II.

The polarity of the electrodes⁶ was reversed every 200 s, then there was a halt of 200–400 s (the UCN beam at the ILL is shared with two other experiments). Two runs with reversed polarity define one measurement cycle j .

We have $L=4$ detectors i . Extending Eq. (6) regarding the number of cycles K and the number of detectors L , we find

$$q_n = \frac{2m_n}{t^2} \frac{1}{LK} \sum_{i=1}^L \sum_{j=1}^K \frac{\Delta n_{i,j}}{\partial_x n_i} \frac{1}{\Delta E_j}. \quad (7)$$

We have $\Delta n_{i,j} = \frac{N_{i,j}^+}{T_{i,j}^+} - \frac{N_{i,j}^-}{T_{i,j}^-}$ with $N_{i,j}$ being the absolute counts and $T_{i,j}$ the measurement time for each detector i in the respective cycle j . The indices $+/-$ denote the polarity of the electrodes. For “+” the left electrode in Fig. 4 has a positive voltage and the right electrode a negative voltage and for “-” vice versa. $\Delta E_j = E_j^+ - E_j^-$ is the difference of the electric field after polarity reversal.

⁶The potential of the electrodes was not as high as achieved in earlier tests ($\Delta E \approx 3.2 \frac{\text{MV}}{\text{m}}$) due to contaminations of the electrode surfaces with Fomblin.

TABLE II. Relevant parameters of the charge measurement during the beam time at the Institut Laue-Langevin in Grenoble, France.

Parameters	Value
Mean time of flight t in the field E	$t = (0.70 \pm 0.20) \text{ s}$
Neutron fluxes in bias points	$n_1 = 19 \frac{1}{\text{s}}, n_2 = 53 \frac{1}{\text{s}},$ $n_3 = 57 \frac{1}{\text{s}}, n_4 = 40 \frac{1}{\text{s}}$
Electric field difference ΔE	$1.2 \frac{\text{MV}}{\text{m}}$
Dimensions of gratings	0.4 mm slit width, 1.1 mm spacing
Slopes of modulation curves	$\partial_x n_1 = -6273 \frac{1}{\text{s}\cdot\text{m}},$ $\partial_x n_2 = -37173 \frac{1}{\text{s}\cdot\text{m}},$ $\partial_x n_3 = 45820 \frac{1}{\text{s}\cdot\text{m}},$ $\partial_x n_4 = 44563 \frac{1}{\text{s}\cdot\text{m}}$
Overall measurement time	$\tau = 3.44 \times 10^5 \text{ s}$
Overall statistical sensitivity	$2.4 \times 10^{-20} \frac{e}{\sqrt{\text{d}}}$

The overall statistical uncertainty of q_n amounts to

$$\delta q_n = \frac{2m_n}{t^2} \frac{1}{LK} \sqrt{\sum_{i=1}^L \sum_{j=1}^K \left(\frac{N_{i,j}^+}{T_{i,j}^{+2}} + \frac{N_{i,j}^-}{T_{i,j}^{-2}} \right) \frac{1}{\partial_x n_i^2} \frac{1}{\Delta E_j^2}}. \quad (8)$$

The overall systematic uncertainty consists of three main uncertainties. The uncertainty of the slopes in the working points,

$$\delta q_{n,\partial_x n} = \frac{2m_n}{t^2} \frac{1}{LK} \sqrt{\sum_{i=1}^L \left(\sum_{j=1}^K \frac{\Delta n_{i,j}}{\partial_x n_i} \frac{1}{\Delta E_j} \right)^2 \left(\frac{\delta(\partial_x n_i)}{\partial_x n_i} \right)^2}, \quad (9)$$

the uncertainty of the electric field,

$$\delta q_{n,E} = \frac{2m_n}{t^2} \frac{1}{LK} \sqrt{\sum_{i=1}^L \sum_{j=1}^K \left(\frac{\Delta n_{i,j}}{\partial_x n_i} \frac{1}{\Delta E_j} \right)^2 \left(\frac{\delta(\Delta E_j)}{\Delta E_j} \right)^2}, \quad (10)$$

and the uncertainty of the mean time of flight,

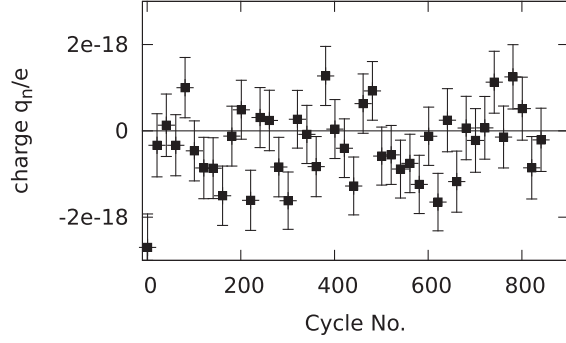
$$\delta q_{n,t} = q_n \frac{2\delta t}{t}. \quad (11)$$

Figure 6 shows the electric neutron charge of every 20th cycle. The cycles show a negative average.

After $K = 840$ cycles, we found

$$q_n = (-1.82 \pm 0.24_{\text{stat}} \pm 0.09_{\partial_x n} \pm 0.02_E \pm 0.78_t) \times 10^{-19} e. \quad (12)$$

Regarding Eq. (5), this corresponds to a shift of the neutron image of

FIG. 6. Measured charge of every 20th cycle in fractions of e .

$$\Delta x = (-4.97 \pm 0.65_{\text{stat}} \pm 0.24_{\partial_x, n}) \times 10^{-6} \text{ m}. \quad (13)$$

The shifts of every single detector can be found in the Supplemental Material [34]. Compared to former results (see Fig. 2), it is obvious that we have had one or more systematic effects, resulting in a significant charge effect. We investigated several possible systematic effects that could have contributed to the measured charge.

C. Discussion of systematic effects

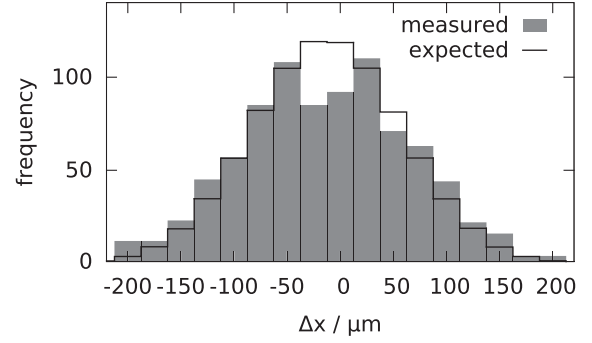
A spatial deflection of the neutrons manifests itself in a change in count rates in every cycle (switching the polarity of the electric field from “+” to “-” and vice versa). A histogram of the spatial deflections $\Delta x_{1,j} = \frac{\Delta n_{1,j}}{\partial_x n_1}$ over all cycles j of the neutrons hitting detector 1 is shown in Fig. 7. One can see a deviation between the measured histogram (grey boxes) of deflections and the expected histogram (solid line). We performed a χ^2 -test for all Δx values over all cycles to compare their distribution with the expected statistical uncertainties for every single detector i :

$$\chi_{\text{red}}^2(di) = \frac{1}{K-1} \sum_{j=1}^K \frac{(\Delta x_{i,j} - \Delta x_i)^2}{(\delta \Delta x_{\text{stati},j})^2}. \quad (14)$$

The indices are equivalent to those in Eq. (7) with $\Delta x_i = \frac{1}{K} \sum_{j=1}^K \Delta x_{i,j}$. $\delta \Delta x_{\text{stati},j}$ denotes the statistical uncertainty of detector i in cycle j . We found a reduced χ^2 of $\chi_{\text{red}}^2(d1) = 1.34$ for detector 1 and 1.00–1.07 for detectors (2)–(4). This is an indication of systematic effects regarding detector 1 at least.

We investigated, among others, the following:

- (1) *The effect of discharges of the electrodes:* As our detectors contain photomultiplier tubes, they are sensitive to discharge light of the electrodes. The probability of discharges in vacuum depends on the polarity of the electrodes. Thus, discharge light might be superimposed to the neutron signals in the detectors and mimic a neutron charge. We closed the UCN shutter from the turbine and continued the measurements without UCN for 39 cycles. The photomultiplier tubes only detected background radiation and occasionally discharge light. We found

FIG. 7. Measured spatial deflections $\Delta x_{1,j}$ for detector 1 over all cycles j (gray boxes) compared to the expected deflection from the known count rate (solid line).

a nonsignificant “mimic shift” of the image of $\Delta x = (-1.10 \pm 3.08_{\text{stat}} \pm 0.31_{\partial_x, n}) \times 10^{-6} \text{ m}$.

- (2) *Movement of optical parts in the electric field:* Residual fields of the electric field could apply stresses to the optical parts (gratings and cylindrical mirror). This effect should even out in a differential measurement if the absolute electrical potential on both electrodes is identical after polarity reversal, because the electric force on grounded objects is independent of the polarity. We closed the UCN shutter from the turbine and placed a blinking light emitting diode in the input guide. We were then able to determine the behavior of the gratings and the cylindrical mirror in the electric field with light. A significant shift of the image in the electric field after polarity reversal for the upper grating (detectors (d 1)–(d 2)) by $(-1.85 \pm 0.36) \times 10^{-6} \text{ m}$ and no significant shift for the lower grating (detectors (d 3)–(d 4)) by $(-0.09 \pm 0.88) \times 10^{-6} \text{ m}$ was detected. This is an indication that we had an asymmetry in the absolute values of the electric voltage between negative and positive polarity. Comparing the shifts of the gratings in the electric fields with our result with UCN in Eq. (13), reveals that this effect only explains a part of our original result.
 - (3) *The behavior of the Fomblin surface in the electric field:* Most of the UCN are reflected by the Fomblin surface. If the shape of the modulation curves in Fig. 5 depends on the polarity, a distortion of the Fomblin surface by the electric field is very likely. The shape of the modulation curves of detectors (d 1)–(d 4) were measured for the polarity “+”, “-” and without an electric field. We compared the curves for each detector. No change could be noticed for (d 2)–(d 4), but the curve for (d 1) was disturbed drastically, especially at the bias point. This explains the larger reduced $\chi_{\text{red}}^2(\Delta x_{d1})$ in comparison to the other detectors. Thus, we omitted (d 1) for the following analysis.
- Points (2) and (3) in the above list are hints that we had systematic effects due to the polarity reversal of the electric field. But electrostatic forces on dielectrics or grounded

objects are independent of the polarity. Thus, an asymmetry of the absolute potential of both electrodes is the most possible explanation for these effects. This would also affect the Fomblin surface: The dielectric force density acting on a dielectric liquid is

$$\vec{f}_D = (\vec{p} \cdot \vec{\nabla}) \vec{E}, \quad (15)$$

with the electric dipole density of the liquid $\vec{p} = \epsilon_0(\epsilon_r - 1)\vec{E}$. ϵ_r denotes the relative permittivity of the liquid ($\epsilon_r \approx 2.4$ for the used Fomblin oil). We simulated the stationary behavior of the Fomblin surface $SF(x)$ in the z direction in the electric field for different asymmetries. The results are shown in Fig. 8.

For an easier mathematical treatment of the Fomblin surface distortions, we define the effective tilt of the surface α_{eff} ,

$$\alpha_{\text{eff}}^{+/-} = \frac{1}{x_r - x_l} \int_{x_l}^{x_r} \frac{dSF^{+/-}(x)}{dx} \Omega(x) dx, \quad (16)$$

with the surface distortion $SF(x)^{+/-}$ under the respective polarity of the electrodes and the normalized distribution of neutrons in the x direction $\Omega(x)$. $\Omega(x)$ is calculated through Monte Carlo simulations. The tilt differences $\Delta\alpha = \alpha_{\text{eff}}^+ - \alpha_{\text{eff}}^-$ under field reversal are shown in Table III.

If we assume a tilt difference of the horizontal mirror between the respective polarities to be the main reason for the remaining pseudocharge, we can approximately calculate the tilt by (see [17]):

$$\Delta F = \Delta E q_{\text{pseudo}} = m_n g \sin \Delta\alpha. \quad (17)$$

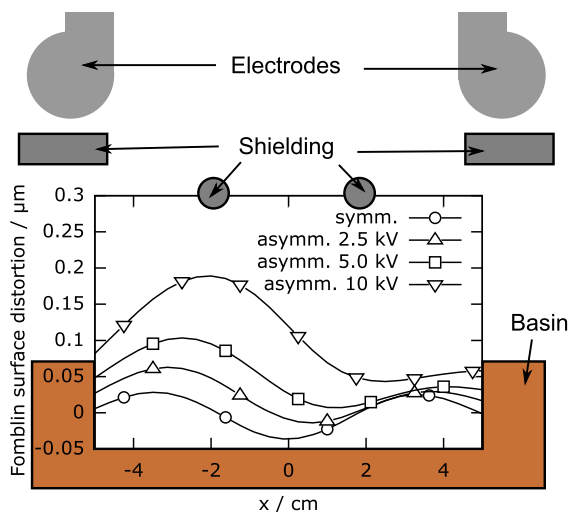


FIG. 8. Displacement of the Fomblin surface $SF^+(x)$ in the z direction in μm for different field configurations. In this example, the left electrode is clamped to $+30$ kV. The potential of the right electrode is $-30, -27.5, \dots$ kV. For $SF^-(x)$ (not shown), the right electrode is clamped to $+30$ kV. $SF^-(x)$ looks like $SF^+(x)$, mirrored horizontally around $x = 0$ cm. The shieldings and the basin (not to scale) have ground potential.

TABLE III. Calculated effective tilts of the Fomblin surface for different field configurations.

Label	Negative potential	$\Delta\alpha_{\text{eff}}$
Symmetric	-30.0 kV	$0.08 \mu\text{rad}^a$
Asymmetric	-27.5 kV	$0.74 \mu\text{rad}$
Asymmetric	-25.0 kV	$1.46 \mu\text{rad}$
Asymmetric	-20.0 kV	$2.56 \mu\text{rad}$

^aThis value is nonzero because $\Omega(x)$ is not symmetric.

This is the projection of the gravitational field on the tilted surface of the horizontal mirror. Subtracting the effect of the movement of the gratings in the electric field from our result in Eq. (12) and omitting detector 1, we find $\Delta\alpha \approx 1.5 \mu\text{rad}$. If we compare this to the tilts in Table III of the Fomblin surface, we find that an asymmetry of ≈ 5 kV must have caused this tilt. The cause for the asymmetry remains unclear. A defect in one of the power lines (positive or negative) of the mechanical high voltage switch seems to be the most likely cause. A gap of about one millimeter could have served as spark gap, resulting in a voltage drop by several kV.

We performed a Monte Carlo simulation of our experiment with such a distorted horizontal mirror. We found shifts of $\Delta x \approx -3.5 \mu\text{m}$ for detector positions 2–4 (for details see Supplemental Material at [34] for Δx and corrections for every detector). By subtracting the systematic effects discussed above from the result in Eq. (12), i.e., the movement of optical components and the assumed tilt of the Fomblin surface, and by omitting detector 1, the remaining charge is given by

$$q_n = (-0.32 \pm 1.22_{\text{stat}} \pm 0.39_{\partial_x n} \pm 0.10_E \pm 0.14_t \pm 1.89_{x_{\text{corr}}} \times 10^{-20} e, \quad (18)$$

which is consistent with earlier measurements (see Sec. II A). The budget of uncertainties is expanded by the uncertainty of this subtraction x_{corr} .

D. Summary and conclusions

During the beam time in 2014, we tested our apparatus the first time for the determination of the free neutron charge. We observed that this apparatus showed a somewhat complicated behavior that caused tiny shifts of the neutron beam. With dedicated measurements we were able to determine these systematic effects. The main reason for the effects was an asymmetry in the absolute potential between both electrodes. This asymmetric potential caused a movement of the gratings

⁷We converted the overall uncertainties of Δx_{corr} given in the Supplemental Material [34] into an uncertainty of q_n using Eq. (7).

and the Fomblin in the residual fields. For future experiments it is crucial to reduce and monitor the influence of systematic effects. This can be done by installing a rigid horizontal mirror, monitoring its tilt during the measurements and independent mechanical mounting of the shielding electrodes from the optics. Then, the maximal possible statistical sensitivity of the apparatus of

$$\delta q_n \approx 1 \times 10^{-21} \frac{e}{\sqrt{\text{day}}} \quad (19)$$

could be reached with higher electric fields, smaller slit widths and reduced background (for a more detailed discussion see [23]). Thus, a new smaller upper bound for the neutron electric charge could be achieved within a few days of measurement with this setup.

ACKNOWLEDGMENTS

We are indebted to the Institute Laue-Langevin, the mechanical workshop of the Institute of Nuclear Chemistry, and T. Brenner (Institute Laue-Langevin) for his enthusiastic help during our beam time in 2014. We also wish to thank B. Lauss (Paul Scherrer Institute, Switzerland) for putting scientific supplies at our disposal and P. Iaydjiev (Institute for Nuclear Research and Nuclear Energy, Bulgaria) and the unknown referee for fruitful discussions. This work is funded by the Deutsche Forschungsgemeinschaft (DFG), German Research Foundation Priority Programme (SPP) 1491 ‘‘Precision Experiments in Particle and Astrophysics with Cold and Ultracold Neutrons.’’ C. S. was a recipient of a fellowship through GRK Symmetry Breaking (DFG/GRK 1581).

-
- [1] J. D. Jackson, *Klassische Elektrodynamik* (De Gruyter, Berlin, 2002).
- [2] P. A. M. Dirac, The theory of magnetic poles, *Phys. Rev.* **74**, 817 (1948).
- [3] R. Foot and R. R. Volkas, Do the SuperKamiokande atmospheric neutrino results explain electric charge quantization?, *Phys. Rev. D* **59**, 097301 (1999).
- [4] J. Beringer *et al.* (Particle Data Group), Review of particle physics (statistics), *Phys. Rev. D* **86**, 010001 (2012).
- [5] R. Foot, Electric charge quantization without anomalies?, *Phys. Rev. D* **49**, 3617 (1994).
- [6] S. L. Adler, Axial-vector vertex in spinor electrodynamics, *Phys. Rev.* **177**, 2426 (1969).
- [7] W. A. Bardeen, Anomalous ward identities in spinor field theories, *Phys. Rev.* **184**, 1848 (1969).
- [8] M. E. Peskin and D. V. Schroeder, *An Introduction to Quantum Field Theory* (Westview Press, Boulder, CO, 1995).
- [9] K. S. Babu and R. N. Mohapatra, Is There a Connection between Quantization of Electric Charge and a Majorana Neutrino?, *Phys. Rev. Lett.* **63**, 938 (1989).
- [10] K. S. Babu and R. R. Volkas, Bounds on minicharged neutrinos in the minimal standard model, *Phys. Rev. D* **46**, R2764 (1992).
- [11] M. Marinelli and G. Morpurgo, The electric neutrality of matter: a summary, *Phys. Lett. B* **137**, 439 (1984).
- [12] P. I. Dee, Attempts to detect the interaction of neutrons with electrons, *Proc. R. Soc. A* **136**, 727 (1932).
- [13] M. Hamermesh, G. R. Ringo, and A. Wattenberg, A measurement of the electron-neutron interaction., *Phys. Rev.* **85**, 483 (1952).
- [14] I. S. Shapiro and I. V. Estulin, Concerning the electric charge of the neutron, *JETP* **30**, 579 (1956).
- [15] C. G. Shull, K. W. Billman, and F. A. Wedgwood, Experimental limit for the neutron charge, *Phys. Rev.* **153**, 1415 (1967).
- [16] R. Gähler, J. Kalus, and W. Mampe, Experimental limit for the charge of the free neutron, *Phys. Rev. D* **25**, 2887 (1982).
- [17] Y. Borisov, N. V. Borovikova, A. V. Vasilev, L. A. Grigoreva, S. N. Ivanov, N. T. Kahukeev, V. V. Nesvizhevsky, A. P. Serebrov, and P. S. Yaidzhiev, On the feasibility of using ultracold neutrons to measure the electric charge of the neutron, *Zh. Tekh. Fiz.* **58**, 951 (1988).
- [18] J. Baumann, R. Gähler, J. Kalus, and W. Mampe, Experimental limit for the charge of the free neutron, *Phys. Rev. D* **37**, 3107 (1988).
- [19] G. Bressi, G. Carugno, F. D. Valle, G. Galeazzi, G. Ruoso, and G. Sartori, Testing the neutrality of matter by acoustic means in a spherical resonator, *Phys. Rev. A* **83**, 052101 (2011).
- [20] G. Barbiellini and G. Cocconi, Electric charge of the neutrinos from SN1987A, *Nature (London)* **329**, 21 (1987).
- [21] V. V. Voronin, L. A. Akselrod, V. N. Zabenkin, and I. A. Kuznetsov, New approach to test a neutron electroneutrality by the spin interferometry technique, *Phys. Procedia* **42**, 25 (2013).
- [22] K. Durstberger-Rennhofer, T. Jenke, and H. Abele, Probing the neutrons electric neutrality with Ramsey spectroscopy of gravitational quantum states of ultracold neutrons, *Phys. Rev. D* **84**, 036004 (2011).
- [23] C. Siemensen, D. Brose, L. Böhmer, P. Geltenbort, and C. Plonka-Spehr, Improved instrument for the determination of the neutron electric charge, *Nucl. Instrum Methods Phys. Res., Sect. A* **778**, 26 (2015).
- [24] C. S. Unnikrishnan and G. T. Gillies, The electrical neutrality of atoms and of bulk matter, *Metrologia* **41**, S125 (2004).
- [25] A. Arvanitaki, S. Dimopoulos, A. Geraci, J. Hogan, and M. Kasevich, How to Test Atom and Neutron Neutrality with Atom Interferometry, *Phys. Rev. Lett.* **100**, 120407 (2008).

- [26] R. Golub, D. Richardson, and S. K. Lamoreaux, *Ultra-Cold Neutrons* (Taylor & Francis, London, 1991).
- [27] W. Mampe, P. Ageron, C. Bates, J. M. Pendlebury, and A. Steyerl, Neutron Lifetime Measured with Stored Ultracold Neutrons, *Phys. Rev. Lett.* **63**, 593 (1989).
- [28] J. M. Pendlebury *et al.*, Revised experimental upper limit on the electric dipole moment of the neutron, *Phys. Rev. D* **92**, 092003 (2015).
- [29] A. Steyerl, H. Nagel, F.-X. Schreiber, K.-A. Steinhauser, R. Gähler, W. Gläser, P. Ageron, J. M. Astruc, W. Drexel, G. Gervais, and W. Mampe, A new source of cold and ultracold neutrons, *Phys. Lett. A* **116**, 347 (1986).
- [30] C. Plonka-Spehr, A. Kraft, P. Iaydjiev, J. Klepp, V. V. Nesvizhevsky, P. Geltenbort, and Th. Lauer, An optical device for ultra-cold neutrons—investigation of systematic effects and applications, *Nucl. Instrum. Methods Phys. Res., Sect. A* **618**, 239 (2010).
- [31] P. Ageron, W. Mampe, and J. C. Bates, UCN storage in fluid walled bottles: A method for a neutron lifetime measurement., *Nucl. Instrum. Methods Phys. Res., Sect. A* **249**, 261 (1986).
- [32] Solexis, Fomblin® PFPE Lubes for Vacuum Applications, 2017, 2004, https://www.solvay.com/en/binaries/Fomblin-PFPE-Lubes-for-Vacuum-Applications_EN-v2.7-229544.pdf.
- [33] F.E. Spada and D. Basov, Fourier transform infrared investigation of thin perfluoropolyether films exposed to electric fields, *Tribol. Lett.* **8**, 179 (2000).
- [34] See Supplemental Material <http://link.aps.org/supplemental/10.1103/PhysRevD.97.052004> for measured Δx and respective corrections for detectors 1–4.